Selective inhibition of tumor microvascular permeability by cavtratin blocks tumor progression in mice

Jean-Philippe Gratton,[1,2,5,6] Michelle I. Lin,[1,2,5] Jun Yu,[1,2] Erik D. Weiss,[1,2] Zao Li Jiang,[1] Todd A. Fairchild,[1,2] Yasuko Iwakiri,[4] Roberto Groszmann,[4] Kevin P. Claffey,[3] Yung-Chi Cheng,[1] and William C. Sessa[1,2,*]

[1]Department of Pharmacology
[2]Vascular Cell Signaling and Therapeutics Program
Boyer Center for Molecular Medicine, Yale University School of Medicine, 295 Congress Avenue, New Haven, Connecticut 06536
[3]Department of Physiology, University of Connecticut Health Center, Farmington, Connecticut 06030
[4]Division of Digestive Diseases, Yale University School of Medicine, 333 Cedar Street, New Haven, Connecticut 06536
[5]These authors contributed equally to this work.
[6]Present address: Institut de Recherches Cliniques de Montréal (IRCM), 110 des Pins Ouest, Montreal, QC, H2W 1R7, Canada.
*Correspondence: william.sessa@yale.edu

Summary

Tumor vasculature is hyperpermeable to macromolecules compared to normal vasculature; however, the relationship between tumor hyperpermeability and tumor progression is poorly understood. Here we show that a cell-permeable peptide derived from caveolin-1, termed cavtratin, reduces microvascular hyperpermeability and delays tumor progression in mice. These antipermeability and antitumor actions of cavtratin occur in the absence of direct cytostatic or antiangiogenic effects. Cavtratin blocks microvascular permeability by inhibiting endothelial nitric oxide synthase (eNOS), as the antipermeability and antitumor actions of cavtratin are markedly diminished in eNOS knockout mice. Our results support the concepts that hyperpermeability of tumor blood vessels contributes to tumor progression and that blockade of eNOS may be exploited as a novel target for antitumor therapy.

Introduction

Vascular endothelial growth factor (VEGF) is a multifunctional cytokine secreted by tumor cells and is thought to be responsible for the hyperpermeable state of tumor blood vessels (Carmeliet and Collen, 2000; Dvorak et al., 1991; Matsumoto and Claesson-Welsh, 2001). VEGF binds to its cognate receptors and can activate the production of the free radical gas nitric oxide (NO) through the enzyme endothelial nitric oxide synthase (eNOS) (Papapetropoulos et al., 1997; Ziche et al., 1997). The stimulated release of NO is central to the in vivo biological activity of VEGF in postnatal animals since VEGF-driven vascular leakage and arteriogenesis/angiogenesis are markedly reduced in eNOS-deficient mice (Fukumura et al., 2001; Murohara et al., 1998a). This increase in tumor vessel permeability is thought to contribute to the deposition of plasma proteins, which may provide a provisional matrix for the inward migration of fibroblasts and endothelial cells into tumors and amplify the signals important for tumor growth. Although the increased extravasation of macromolecules is an established property of tumor vessels (Dvorak et al., 1988), it has never been exploited as a target for antitumor therapy.

Recently, we reported that a cell-permeable peptide, consisting of the homeodomain of the *Drosophila* transcription factor antennapedia (AP or penetratin), coupled to a peptide derived from the eNOS inhibitory protein caveolin-1 (AP-Cav) was able to selectively block endothelium-dependent relaxations and eNOS, but not inducible NOS (iNOS) mediated NO release (Bucci et al., 2000). This peptide, now termed cavtratin (see Supplemental Table S1 at http://www.cancercell.org/cgi/content/full/4/1/31/DC1), when administered to mice markedly reduced interstitial edema and microvascular leakage in the context of two models of subchronic inflammation but did not influence systemic hemodynamics (Bucci et al., 2000). In the present study, we investigated whether cavtratin, by virtue of its ability to reduce interstitial edema, could influence vascular leakage in tumors and impact tumor progression in mice.

Results and Discussion

Since hyperpermeability has long been recognized as a hallmark of tumor vasculature (Dvorak et al., 1988), we examined the

SIGNIFICANCE

The leakiness to plasma macromolecules has long been recognized as a trait of tumor microvasculature. The impact of this phenomenon has not been exploited in the context of tumor growth and maintenance or for the development of novel therapies. Our study shows that a selective inhibitor of nitric oxide-dependent vascular leakage, cavtratin, reduces plasma macromolecule extravasation from tumor vasculature. This reduced tumor vessel permeability results in a significant inhibition of tumor growth in two mouse models. Thus, cavtratin is a novel therapeutic modality that directly interferes with vessel permeability, a hallmark of tumor vasculature necessary for tumor maintenance and growth in mice.

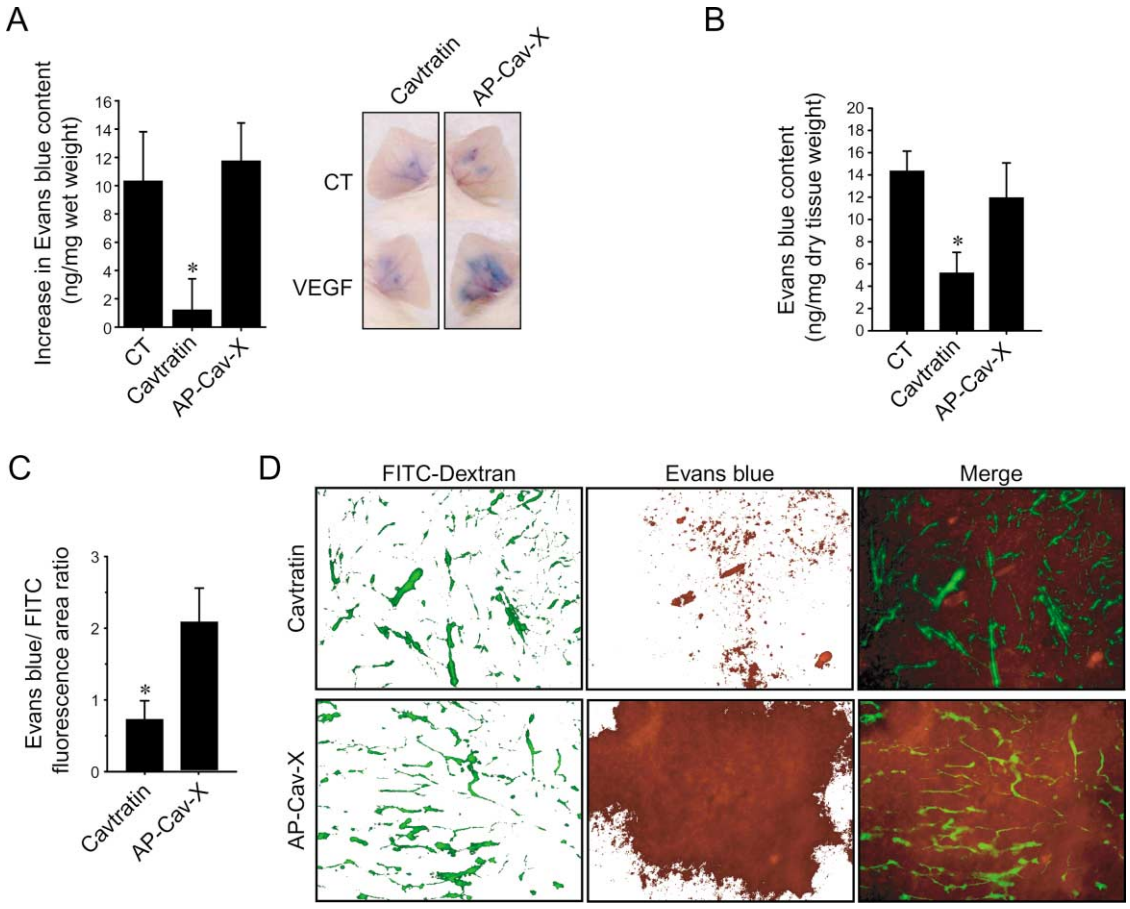

Figure 1. Cavtratin reduces VEGF-induced and tumor vascular permeability

A: VEGF-mediated vascular leakage was monitored by intradermal injection of VEGF (30 ng) into the ear of CD-1 mice. Mice were treated with vehicle, cavtratin, or AP-Cav-X (2.5 mg/kg i.p. each) for 45 min and were then anesthetized (ketamine/xylazine) for administration of Evans blue (via the left jugular vein; 30 mg/kg) 1 min prior to VEGF (30 ng in 30 μl) and saline (30 μl) administration. VEGF and saline were each administered intradermally (for 30 min) on the dorsal side of each ear. Ears were weighed prior to extraction of Evans blue with formamide and the content of Evans blue was determined spectrophotometrically at 610 nm.

B: C57BL/6 mice bearing LLC tumors of 2500 mm^3 were treated with vehicle, cavtratin (2.5 mg/kg; i.p.), or AP-Cav-X (2.5 mg/kg; i.p.) 1 hr before Evans blue administration. Tumors were excised and Evans blue content was quantified spectrophotometrically.

C: Animals treated as in **B**, and in addition, FITC-dextran (400 kDa; i.v.) was administered to the mice (100 mg/kg) 1 min prior to tumor excision. One hundred micrometer vibrotome sections were quantified for areas of Evans blue (TRITC/ rhodamine filter) and FITC-dextran fluorescence and expressed as ratios of area of Evans blue to FITC-dextran. All graphs are represented as means ± SEM and *$p \leq 0.05$ versus CT and AP-Cav-X.

D: Representative images of Evans blue (red) and FITC-dextran (green) fluorescence of LLC tumors from cavtratin- and AP-Cav-X-treated mice. All graphs are from at least five mice per group.

effects of cavtratin on vascular leakiness. VEGF is a prominent cytokine responsible for the hyperpermeable state of tumor vessels; thus we initially investigated the effects of cavtratin on VEGF-driven vascular leakage in a modified Miles assay (Figure 1A). Intradermal administration of VEGF in the ear of CD-1 mice produced a marked increase in Evans blue extravasation, which is indicative of albumin and plasma protein leakage into the interstitium (Murohara et al., 1998b). Treatment of mice with 2.5 mg/kg of cavtratin (administered i.p. 30 min prior to intradermal VEGF) resulted in a significant inhibition of vascular leakage compared to vehicle or AP-Cav-X (a scrambled control peptide administered at 2.5 mg/kg; Figure 1A) treated mice. This effect of VEGF is largely dependent on NO release since VEGF-induced vascular leak is abrogated in eNOS-deficient mice or by treatment of wild-type mice with NOS inhibitors, such as L-nitro arginine methyl ester (L-NAME; Fukumura et al., 2001). However, in contradistinction to NOS inhibitors, cavtratin does not affect systemic blood pressure or blood flow. Intravenous administration of cavtratin or AP-Cav-X (2.5 mg/kg, i.v. bolus) had no effect on systemic blood pressure (81.8 ± 3.2 mm Hg versus 83.6 ± 4.1 mm Hg for cavtratin- and AP-Cav-X-treated mice, respectively; $n = 7$ mice per group) consistent with previous data (Bucci et al., 2000).

In order to determine if cavtratin treatment acutely reduced vascular permeability in the tumor vasculature, we monitored the effects of cavtratin on the hyperpermeable state of the tumor vasculature. Lewis lung carcinoma (LLC) tumors inoculated subcutaneously into C57BL/6 mice were allowed to grow to approximately 2500 mm^3, and animals were treated with either vehicle or a single dose of cavtratin or AP-Cav-X (2.5 mg/kg of each). Evans blue was then administrated to the mice (30 mg/kg, i.v.) and the tumors were subsequently perfused with saline and the

amount of Evans blue extravasated into the tumor quantified. Figure 1B shows that acute administration of cavtratin significantly reduced the extravasation of Evans blue into tumors compared to AP-Cav-X-treated animals. However, cavtratin did not reduce basal vascular permeability in the lungs from treated mice (8.8 ± 1.6 ng, 9.1 ± 1.4 ng, and 8.6 ± 1.8 ng Evans blue/mg dry tissue, for cavtratin-, AP-Cav-X-, and vehicle-treated mice, respectively; n = 4).

To further confirm the decreased tumor blood vessel leakiness in cavtratin-treated animals, we quantified the ratio of extravascular albumin (bound to Evans blue as an index of fluid extravasation) to blood vessels in the tumor microcirculation. Mice bearing LLC tumors (approximately 2500 mm^3) were injected with a single dose of cavtratin or AP-Cav-X (2.5. mg/kg of each) followed by intravenous administration of high molecular weight FITC-dextran (to label the vascular compartment) imaged in the FITC filter (Lindsberg et al., 1997) and Evans blue (to label the extravasation of plasma protein in the tumor component) imaged in the TRITC/rhodamine filter (Lindsberg et al., 1997). The ratio of rhodamine/FITC fluorescence in multiple tumor sections was then assessed by optical sectioning of the tumors. The fluorescence ratio of Evans blue to FITC-dextran per tumor sections allows for a direct quantification of the relative extravascular albumin content normalized to the density of blood vessels in the tumor area. As seen in Figure 1C, cavtratin reduced the ratio of rhodamine/FITC fluorescence, indicating that the peptide was blocking vascular leakage in the tumor microcirculation. Representative images of tumor section (Figure 1D) from cavtratin- and AP-Cav-X-treated mice show that for a similar volume of blood vessels (green FITC-dextran fluorescence), a strong decrease in Evans blue fluorescence (red filter) in cavtratin-treated animals is observed compared to AP-Cav-X-treated animals.

To explore the possibility that interfering with vessel permeability had an effect on tumor growth, we examined the effects of cavtratin administration on tumor progression in mice. The human hepatocarcinoma cell line HepG2 (5×10^6 cells per mouse) was injected subcutaneously into the flank of NCr Nude athymic mice and secondly, the mouse-derived LLC cell line (1×10^6 cells per mouse) was dorsally injected to C57BL/6 mice. When the tumors reached a palpable size, mice were randomized into different treatment groups and treated with a single daily dose of cavtratin (2.5.mg/kg/day) given intraperitoneally for the duration of the study. Controls included noninjected, vehicle-injected, or a scrambled control peptide AP-Cav-X that has previously been shown to be ineffective at blocking the NO synthesis (2.5 mg/kg/day; Bucci et al., 2000). In all groups, tumor progression was monitored as fractional tumor volume to reflect the increase in tumor mass per animal (Mauceri et al., 1998). Treatment with vehicle, cavtratin, or AP-Cav-X did not influence normal bodily functions and behavior including weight gain, appetite, or grooming behavior. As seen in Figure 2, cavtratin significantly reduced tumor progression in immunodeficient mice bearing human HepG2 cells tumors and in immunocompetant mice bearing LLC tumors (Figures 2A and 2B). The final tumor volumes were as follows: vehicle: 2802 ± 116 mm^3, cavtratin: 1344 ± 132 mm^3, AP-Cav-X: 2794 ± 213 mm^3 for HepG2 tumors; and vehicle: 3895 ± 618 mm^3, cavtratin: 2385 ± 366 mm^3, and AP-Cav-X: 3943 ± 689 mm^3 for LLC tumors. Treatment with vehicle and the control peptide, AP-Cav-X, were without effect. These data were repeated in three to four separate experiments with at least five mice per group. Histological examination of tumor cross-sections shows that cavtratin-treated tumors had larger areas of necrosis than did AP-Cav-X-treated mice, consistent with tumor cell apoptosis leading to necrosis (Figures 2C and 2D).

Next we examined potential actions of the peptide in tumors. Acute administration of biotinylated cavtratin (10 mg/kg, i.p.) resulted in the appearance of the labeled peptide in the tumor mass (Supplemental Figure S1 on *Cancer Cell* website). Examination of NOS activity after acute injection of cavtratin (2.5.mg/kg, i.p.) reduced tumor-derived NOS activity whereas AP-Cav-X did not (Figure 3A), demonstrating that the peptide could inhibit NOS in the tumor. In addition, 7 day treatment with cavtratin, but not AP-Cav-X, also increased the number of apoptotic cells (indexed by TUNEL staining) in non-necrotic, apparently viable regions of the tumor (Figure 3B). Finally, we examined the extent of angiogenesis in mice bearing the HepG2 tumors by quantifying PECAM-1-positive blood vessels and PECAM-1 protein levels (Figures 3C and 3D). As seen in Figure 3C, PECAM-1-positive profiles were markedly reduced in tumors from cavtratin-treated mice compared to control, vehicle-, and AP-Cav-X-treated animals. In addition, the levels of PECAM-1 protein by Western blotting were markedly reduced in cavtratin-treated mice, whereas VEGF 165 and caveolin-1 levels were identical (Figure 3D). Finally, since both angiogenesis and lymphangiogenesis may be important for tumor progression, we examined lymphatic vasculature using Flt-4 as a generalized marker for lymphatic endothelium (Stacker et al., 2002) in cavtratin- and AP-Cav-X-treated tumors. As seen in Figure 3E, there were fewer Flt-4-positive cells in tumors from cavtratin-treated mice. These data suggest that cavtratin reduces eNOS activity, decreases tumor permeability, and triggers apoptosis leading to a loss of tumor cells, capillaries, and lymphatic vessels.

In order to investigate if the reduction in tumor growth and increased tumor apoptosis/necrosis produced by cavtratin treatment could be due to a direct antiangiogenic effect (i.e., by blocking endothelial cell proliferation, migration, and/or organization) in addition to its effect on vascular leak, we monitored blood vessel formation in a model not associated with vascular leakiness. We implanted Matrigel plugs filled with basic fibroblast growth factor (bFGF) on the back of nude mice and monitored vessel assembly in cavtratin-treated mice (Claffey et al., 2001). The Matrigel model of angiogenesis requires stromal cell formation around the plug followed by massive proteolysis, and the subsequent ingrowth and reorganization of host endothelial cells with support cells including fibroblasts and pericytes to form patent vessels. In Figures 4A and 4B, Matrigel plugs without growth factor showed very few erythrocyte-filled vessels and cell infiltration, in general (Claffey et al., 2001). However, the presence of bFGF triggered a robust angiogenic response, but cavtratin and AP-Cav-X did not influence this process and the vascular profiles were not different amongst the treatment groups, suggesting that cavtratin does not directly suppress angiogenesis, per se.

The effect of cavtratin on endothelial and tumor cell proliferation in culture was also examined. VEGF or serum-induced ^{3}H-thymidine incorporation into DNA of bovine aortic endothelial cells (BAEC) was not affected by the presence of cavtratin or AP-Cav-X (10 μM) in the media (Supplemental Figure S2 on *Cancer Cell* website), although this concentration of cavtratin blocks acetylcholine-induced vasodilation of mouse aortic rings and NO release from endothelial cells (Bucci et al., 2000). This

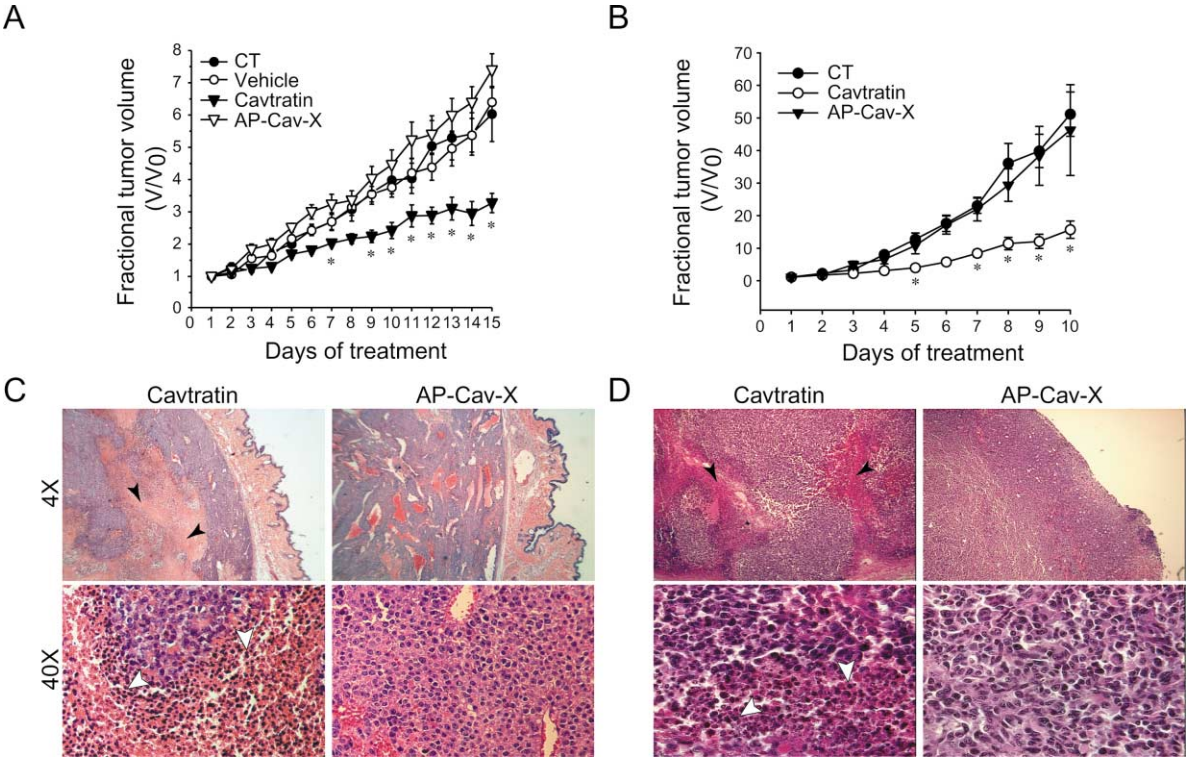

Figure 2. Cavtratin reduces tumor burden

A: Athymic NCr nude mice and **B:** C57BL/6 mice were injected subcutaneously with either human HepG2 hepatocarcinoma or mouse Lewis lung carcinoma (LLC) cells, respectively. Tumors were allowed to grow to ~400 mm^3 for HepG2 and to ~100 mm^3 for LLC before randomization into treatment groups of control, vehicle-, cavtratin-, or AP-Cav-X-treated. Mice were given daily intraperitoneal injections of 2.5 mg/kg of peptides. Tumor volume was determined daily using a caliper and applying the formula (volume = $0.52 \times [\text{width}]^2 \times [\text{length}]$) for approximating the volume of a spheroid. Tumor growth is presented as means ± SEM fraction of the initial tumor volume at day 1 of treatment, n = 7–8 mice per group, *$p \leq 0.05$ when compared to AP-Cav-X treatment. Representative microscopic images, 4× (top panels) and 40× (bottom panels) objectives of HepG2 (**C**) and LLC (**D**) cells tumors stained with hematoxylin and eosin at the end of peptide treatments. Note the presence of necrotic tissue (black arrow head) and condensed nuclei (white arrow head) in cavtratin-treated tumors.

result indicates that endothelial cell proliferation is not influenced by the cell-permeable peptides. We also monitored if tumor cell growth was influenced by cavtratin, thus contributing to the reduced tumor size and necrosis in cavtratin-treated animals. HepG2 cells in culture were grown (10% FBS) in the presence of increasing concentrations of cavtratin and AP-Cav-X (Supplemental Figure S2), and no detectable effect on cell number was observed for both peptides at concentrations up to 10 μM. These results indicate that the inhibition of tumor growth in these mouse models by cavtratin is unrelated to growth factor-driven blood vessel formation, per se, or endothelial cell or tumor cell proliferation.

The above data suggest that cavtratin blocks eNOS-derived NO release (Bucci et al., 2000) and this mechanism contributes to the reduction in tumor leakiness and progression. To directly examine the role of eNOS in vascular leakage, LLC tumors were implanted into C57Bl6 (wt) and congenic $eNOS^{-/-}$ mice and allowed to grow to approximately 2000 mm^3. Animals were then treated with either vehicle or a single dose of cavtratin or AP-Cav-X (2.5 mg/kg of each). Evans blue was then administrated to the mice (30 mg/kg, i.v.) and the tumors were subsequently perfused with saline and the amount of Evans blue extravasated into the tumor quantified. As seen in Figure 5A, tumors in $eNOS^{-/-}$ mice are less permeable to Evans blue compared to tumors in wt mice. More importantly, cavtratin reduced tumor microvascular permeability in wt mice to the same level as that seen in $eNOS^{-/-}$ mice and did not reduce permeability further in tumors implanted into $eNOS^{-/-}$ mice. To examine if the reduction in vascular permeability seen in $eNOS^{-/-}$ mice influences tumor progression and if the diminished effect of the peptide on vascular permeability in $eNOS^{-/-}$ translates into a reduction in tumor size, wt and $eNOS^{-/-}$ were implanted with LLC cells and subgroups of mice treated daily with cavtratin. Tumor progression is markedly reduced in $eNOS^{-/-}$ mice (open circles) compared to LLC implanted into wt mice (solid circles; Figure 5B), an effect associated with a reduction in PECAM-1-positive vascular profiles in the tumors (6.6% ± 0.4% versus 3.5% ± 0.7* % PECAM-1-positive density (arbitrary units) in LLC tumors implanted into wt versus $eNOS^{-/-}$, *$p < 0.05$; n = 4 per group). Daily administration of cavtratin slowed tumor progression in wt mice (solid triangles) but was less efficacious in $eNOS^{-/-}$ mice (open triangles) bearing LLC tumors. These data show that the antipermeability and antitumor effects of cavtratin are markedly reduced in $eNOS^{-/-}$ mice.

Since there is evidence that caveolin-1 may interact with the VEGF receptor, Flk-1 (Labrecque et al., 2003), and negatively regulate c-src, a kinase involved in VEGF-induced permeability (Eliceiri et al., 1999), we examined if cavtratin can influence

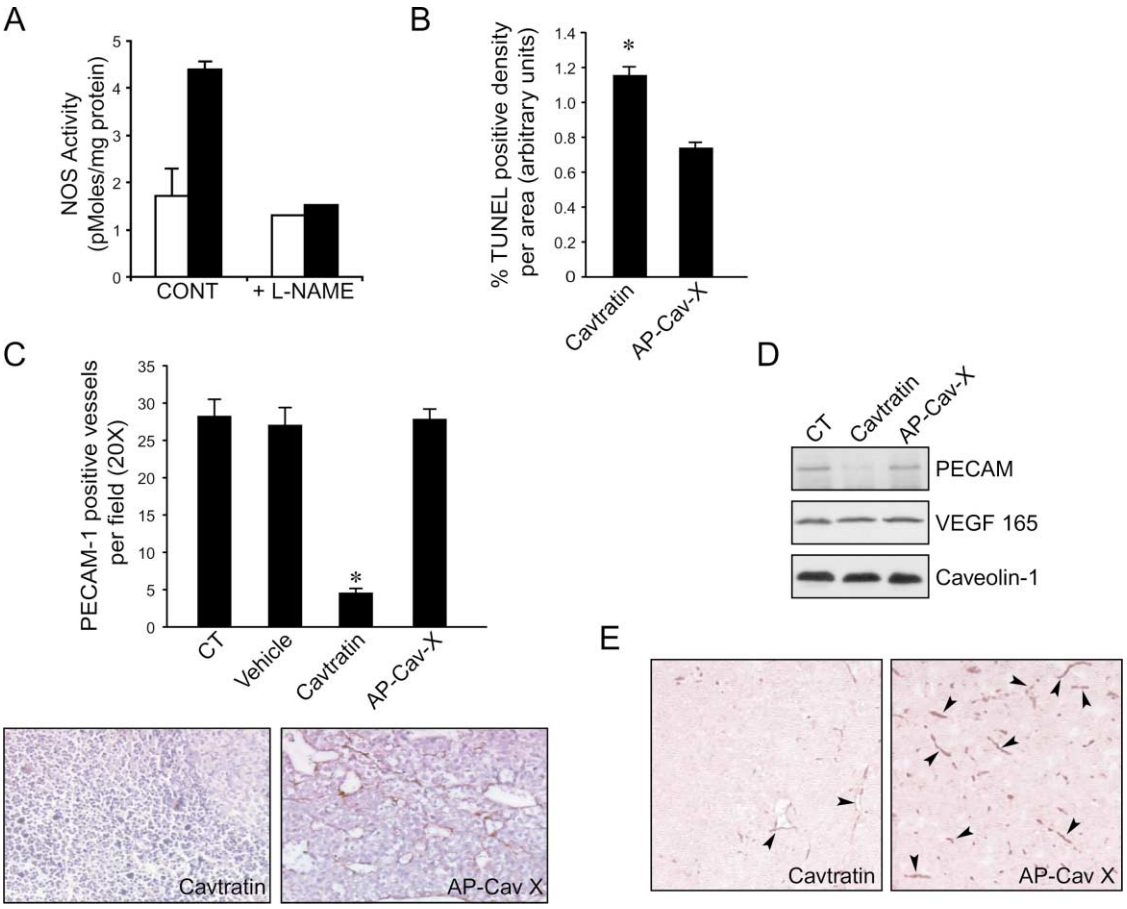

Figure 3. Cavtratin decreases tumor NOS activity, increases apoptosis, and reduces tumor vasculature

A: In vivo treatment with cavtratin (open bars) but not AP-Cav-X (closed bars) reduces tumor NOS activity. eNOS-enriched membranes were prepared and NOS activity assessed by the conversion of [^{14}C] l-arginine to [^{14}C] l-citrulline in vitro. Membrane extracts were also treated with a NOS inhibitor, L-NAME (1 mM) to demonstrate the specificity of the activity assay. Data represented pooled samples from three animals per group and are plotted as mean ± SEM.

B: Cavtratin increases the number of TUNEL-positive cells. Mice bearing LLC tumors were treated daily for 7 days with cavtratin or AP-Cav-X and the number of apoptotic cells assessed histochemically (n = 3 tumors per group with 4 sections quantified per tumor).

C: HepG2 tumors sections from untreated control (CT), vehicle-, cavtratin-, and AP-Cav-X-treated NCr nude mice were immunostained for PECAM-1 and quantified as mean ± SEM of the number of blood vessels in three different 20× fields of view of three different sections from tumors of five different animals per treatment group. *$p \leq 0.05$ when compared to AP-Cav-X treatment. Inset: Representative sections of PECAM-1 immunohistochemistry from cavtratin- and AP-Cav-X-treated animals.

D: Western blot analysis for PECAM-1, VEGF 165, and caveolin-1 levels in tumors after 14 day peptide treatment. Protein extracts (50 μg) were loaded from control (CT), cavtratin-, and AP-Cav-X-treated mice bearing HepG2 tumors.

E: Cavtratin reduces Flt-4-positive cells in tumors.

these pathways, in addition to its effects on eNOS. Treatment of endothelial cells with cavtratin did not block VEGF-induced Flk-1 autophosphorylation (Figure 6A) or influence the levels or extent of phosphorylation of c-src (P^{Y416}-src) and the c-src substrate, caveolin-1 (P^{Y14} cav-1, Figure 6B). In contrast, treatment of endothelial cells with PP2, a c-src inhibitor, reduced P^{Y416}-src and P^{Y14} caveolin-1 levels. Since cavtratin did not directly influence the phosphorylation of c-src or caveolin-1, we examined the effect of cavtratin on the tyrosine phosphorylation of VE-cadherin, a key junctional molecule linked to changes in vascular permeability (Carmeliet et al., 1999). Treatment of human endothelial cells with cavtratin, AP-Cav-X, or a NOS inhibitor, L-NMMA, had no effect on the tyrosine phosphorylation of VE-cadherin. Taken together, these data support the idea that eNOS is a primary molecular target of the peptide and genetic loss of eNOS is comparable to eNOS inhibition by cavtratin.

Collectively, our data demonstrate that cavtratin inhibits eNOS-dependent vascular leakage in established tumors by enhancing tumor apoptosis, decreasing tumor angiogenesis, thereby reducing tumor burden. The mechanisms of how cavtratin reduces vascular leakage most likely relate to the ability of caveolin-1 to serve as a negative regulator of eNOS function (Bucci et al., 2000; Garcia-Cardena et al., 1997; Michel et al., 1997), and NO may influence pathways regulating transcellular and paracellular fluid exchange (Bates et al., 1999; Michel and Curry, 1999; Schubert et al., 2002). The precise molecular mechanisms of how NO influences tumor and postcapillary fluid exchange are not known (i.e., protein kinase G or direct nitrosyla-

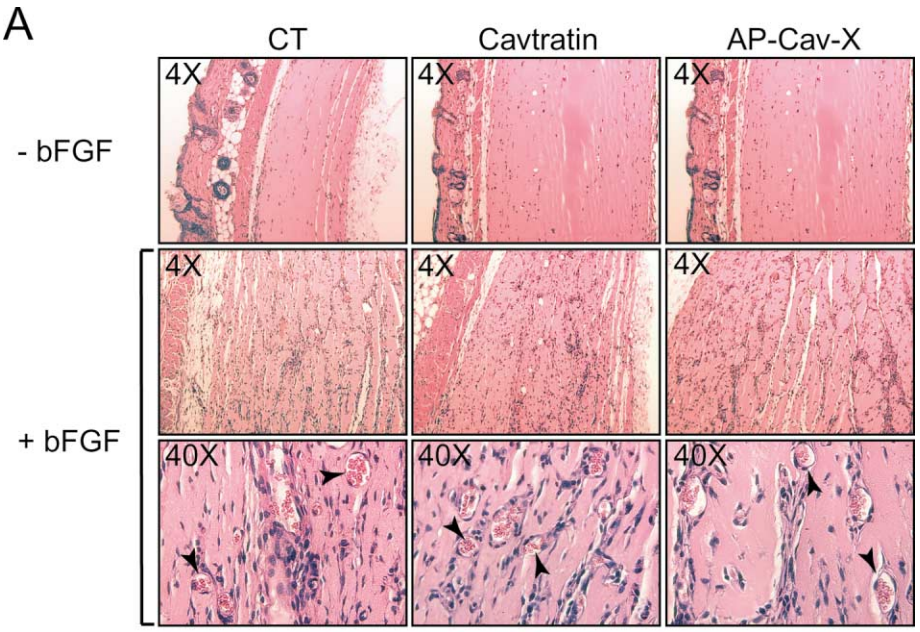

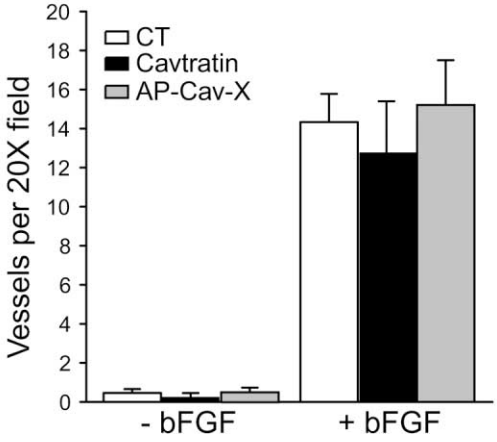

Figure 4. Cavtratin does not block angiogenesis, per se

A: Matrigel plugs containing either vehicle or a mixture of heparin (23.3 μg/ml)/bFGF (0.8 μg/ml) were injected dorsally (right and left center of back) to NCr nude mice. Control mice (CT) or mice, treated with cavtratin or AP-Cav-X (2.5 mg/kg/day) were treated for 10 days before Matrigel plug dissection and tissue section staining with hematoxylin and eosin. Representative section from Matrigel containing saline (top row) or heparin/bFGF (two bottom rows) from control, cavtratin, and AP-Cav-X show similar cell infiltration and erythrocyte-filled blood vessels (arrows). **B:** Quantity (mean ± SEM) of erythrocyte-filled blood vessels in Matrigel plugs from five different animals per group in three different 20× fields of view per section. *$p < 0.05$ when compared to AP-Cav-X treatment.

tion of junctional proteins). However, the reduced effectiveness of cavtratin on tumor permeability and progression in eNOS$^{-/-}$ mice strongly supports the idea that eNOS is required for the actions of cavtratin; however, we cannot rule out the possibilities of other targets for cavtratin leading to a reduction in permeability/progression or that the biodistribution of the injected peptide may differ in tumors implanted into wt and eNOS$^{-/-}$ mice. Another important aspect of our study are data showing that cavtratin is pharmacologically distinct from conventional NOS inhibitors since it does not exert significant hemodymanic effects, administered intravenously (this study) or intraperitoneally (Bucci et al., 2000). The lack of a hemodynamic effect argues against cavtratin simply reducing blood flow and implies that cavtratin targets a fraction of the total eNOS pool that regulates microvascular leakage and permeability changes. Thus, we suggest that cavtratin interferes with tumor growth by locally blocking eNOS in tumor microvasculature, thereby altering the state of tumor vessel permeability which is necessary for tumor cell survival, angiogenesis, and tumor progression in these mouse models. More importantly, our study shows that sole intervention at the level of blocking vessel permeability reduces tumor progression, suggesting that targeting tumor microvascular leakiness may be a novel, unexploited strategy for antitumor therapy.

Experimental procedures

Peptides

Peptides, corresponding to the putative scaffolding domain of caveolin-1 (amino acids 82–101; DGIWKASFTTFTVTKYWFYR) or the scrambled control peptide Cav-X (WGIDKAFFTTSTVTYKWFRY), were synthesized as a fusion peptide to the C terminus of the antennapedia (AP) internalization sequence (RQIKIWFQNRRMKWKK) by standard Fmoc chemistry, purified and analyzed by reversed-phase high-pressure liquid chromatography and mass

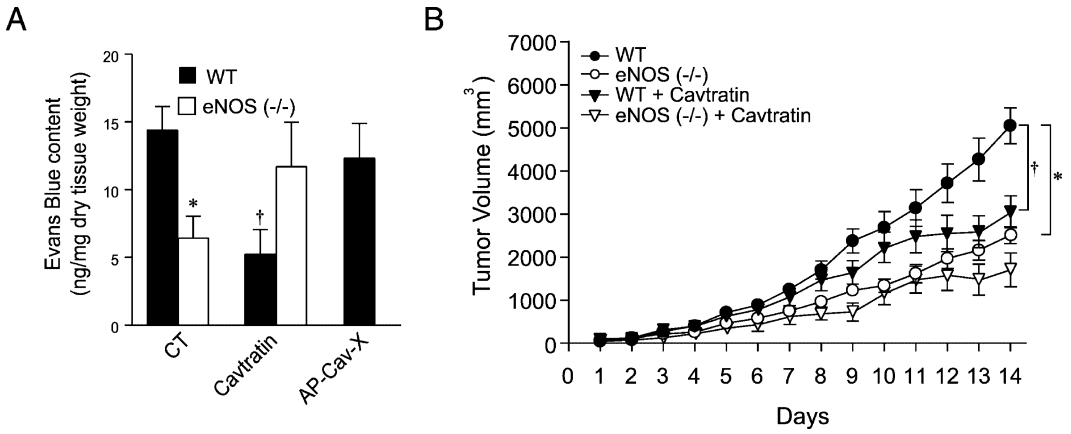

Figure 5. eNOS knockout mice have decreased vascular permeability, tumor growth, and sensitivity to cavtratin

C57BL/6 wild-type (wt) or eNOS$^{-/-}$ mice were injected subcutaneously with mouse Lewis lung carcinoma (LLC) cells.

A: As in Figure 1, mice bearing tumors of approximately 2500 mm^3 were treated with either cavtratin (2.5 mg/kg; i.p.) or AP-Cav-X (2.5 mg/kg; i.p.) or untreated (CT) 1 hr before Evans blue administration. Tumors were excised and Evans blue content was quantified spectrophotometrically (n = 4). *$p < 0.05$ when compared to wt. †$p < 0.05$ when compared to CT.

B: Tumor progression of LLC tumors implanted into wt (●,▼) or eNOS$^{-/-}$ (○,▽). Mice were either untreated (●,○) or treated with cavtratin at 2.5 mg/kg; i.p. (▼, ▽). Tumor volume was determined daily using a caliper as in Figure 2 and was plotted as means ± SEM of tumor volume (n = 9). This experiment was repeated three times with similar results. Tumors in eNOS$^{-/-}$ mice are significantly different from wt mice and cavtratin reduces tumors in wt mice.

spectrometry by the W.M. Keck biotechnology resource center at Yale University School of Medicine. For detection of the cavtratin peptide in vivo, biotin followed by an aminohexanoic acid spacer was added to the amino terminus of the AP fusion peptide. Previous studies in our lab (Bucci et al., 2000) have shown that at least 100 μM of the biotinylated cavtratin was required to demonstrate an inhibitory effect on vascular relaxation. Peptides were dissolved initially in DMSO and diluted 1000-fold in sterile saline before in vivo administration (2.5 mg/kg per animal).

Tumor implantation

HepG2 cells were cultured in MEM containing 2 mM L-glutamine and penicillin/streptomycin (Pen/Strep). LLC cells were cultured in DMEM containing

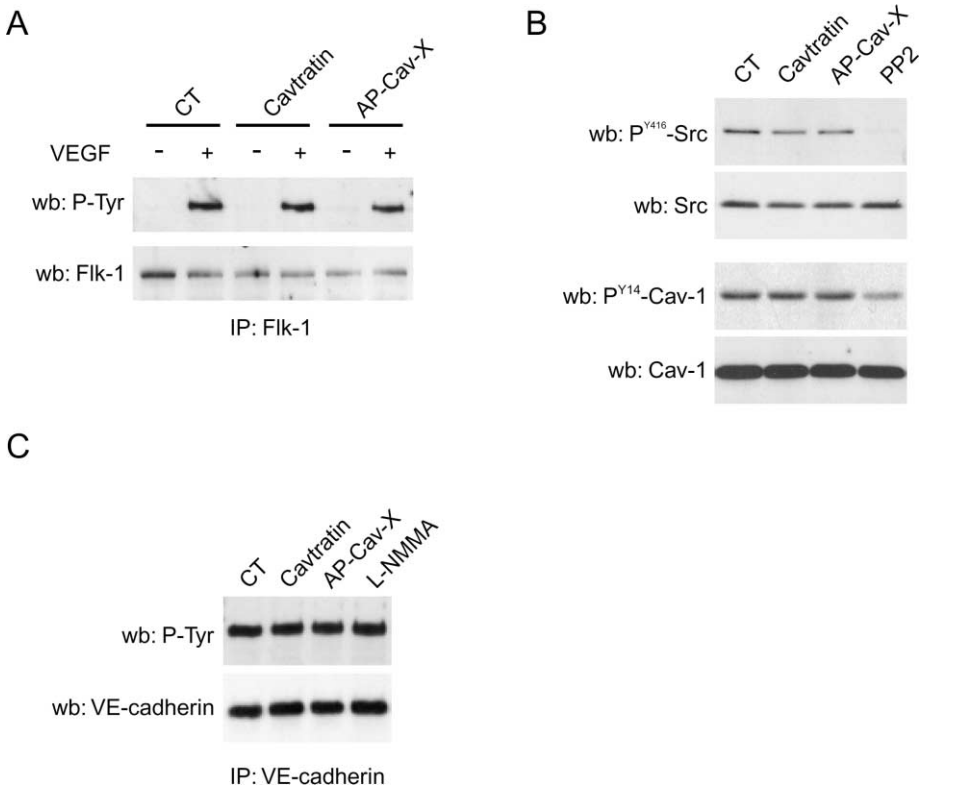

Figure 6. Lack of effect of cavtratin on VEGF receptor phosphorylation, src signaling, or VE-cadherin

In **A**, bovine aortic endothelial cells (BAECs) were treated with vehicle (CT), cavtratin, or AP-Cav-X (10 μM) for 90 min, stimulated with VEGF (10 ng/ml) for 5 min, and Flk-1 immunoprecipitated. Lysates were electrophoresed and samples blotted for tyrosine phosphorylated Flk-1 (P-Tyr) and total Flk-1.

B: BAECs were treated with vehicle (CT), cavtratin, AP-Cav-X (10 μM each), or the src inhibitor PP2 (10 μM) and the levels of P^{Y416} c-src and P^{Y14} caveolin assessed using phospho-state-specific antibodies.

In **C,** human endothelial cells (EA.hy) were treated with vehicle (CT), cavtratin, AP-Cav-X (10 μM each), or L-NMMA (1 mM) for 60 min and VE-cadherin immunoprecipitated. Lysates were electrophoresed and samples blotted for tyrosine phosphorylated VE-cadherin (P-tyr) and total VE-cadherin.

2 mM L-glutamine and Pen/Strep. Tumor cells were grown to 80% confluence on the day of implantation; cells were washed, trypsinized, and resuspended in serum free, L-glutamine and Pen/Strep free DMEM. HepG2 cells (5×10^6 cells in 100 μl) were injected subcutaneously in the left flank of male 6- to 8-week-old NCr nude mice (Taconic, Germantown, New York). LLC cells (1×10^6 cells in 100 μl) were subcutaneously injected on the back of 6- to 8-week-old C57BL/6 mice or congenic eNOS$^{-/-}$ mice (Jackson Laboratory). Mice were given 2.5 mg/kg of peptides daily by intraperitoneal injections. Tumor volume was determined daily using a caliper and applying the formula (volume = $0.52 \times$ [width]$^2 \times$ [length]) to approximate the volume of a spheroid.

Mean arterial pressure measurement

C57BL/6 mice were weighed and anesthetized with ketamine hydrochloride (100 mg/kg) and fastened to a surgical board. Mean arterial pressure (MAP) was measured by cannulating the exposed left femoral artery with a PE-10 (intravascular) catheter joined to PE-50 (extravascular) polyethylene tubing (Clay Adams, Becton Dickinson, Parsippany, New Jersey), connected to a H-P pressure transducer (Hewlett-Packard, Andover, Massachusetts). MAP was measured acutely and 60 min after bolus injection of cavtratin or AP-Cav-X peptides (2.5 mg/kg) through the jugular vein (n = 7 each).

Immunohistochemistry

Tumors were harvested and fixed in 10% formalin for 1–2 hr and transferred to 70% ethanol overnight followed by paraffin embedding. These tissues were sectioned for hematoxylin and eosin staining. For immunohistochemical staining, 3% paraformaldehyde fixed tumor tissues were frozen in OCT after overnight dehydration in 30% sucrose in PBS. Five micrometer sections were stained for PECAM-1 (Pharmingen) or Flt-4 (R&D Systems) and visualized using the Vectastain ABC kit (Vector laboratories) followed by incubation with NovaRed substrate (Vector laboratories). For the detection of biotinylated cavtratin, 10 μm tumor sections were stained for Alexa 488 conjugated Steptavidin and counterstained with DAPI.

TUNEL assay

After 7 days of peptide treatment, C57BL/6 mice bearing LLC tumors were sacrificed and tumor tissue processed for paraffin embedding as mentioned above. Five micrometer sections were deparaffinized and digested with 20 ug/ml of Proteinase K for 15 min. After quenching endogenous peroxidase activity using 3% H_2O_2 for 5 min, these sections were incubated with ApoTag TUNEL (Intergen) reaction solution for 1 hr at 37°C. TUNEL-positive nuclei were then processed for immunoperoxidase staining with anti-digoxigenin antibody and visualized by NovaRed substrate. The percent of TUNEL-positive nuclei was quantified using Scion Image 1.62c (Scion Corporation) and normalized to total pixel density of non-necrotic areas that were quantified.

Endothelial cell proliferation

Bovine aortic endothelial cells (BAECs) were cultured in DMEM containing 10% FBS (HyClone), containing 2 mM L-glutamine and Pen/Strep. Cells were plated in 96 well plates (5000 cells/well) and serum starved for 24 hr. Peptides were added 1 hr before VEGF or 5% FBS stimulation. Growth factor-stimulated BAEC proliferation was monitored for 20 hr, [^{3}H]-thymidine (0.5 μCi/well) was present for the last 4 hr. Nuclear DNA was extracted using a Brandel Harvester 96 onto Whatman GF/B paper filter mats. The filters were assayed for ^{3}H using a Beckman model LS6000IC liquid scintillation counter.

Miles assay

Male Swiss mice (CD-1, 25–30 grams) were pretreated for 45 min with vehicle, cavtratin, or AP-Cav-X (2.5 mg/kg i.p. each). Animals were anesthetized with ketamine/xylazine, and a catheter was introduced into the left jugular vein for administration of Evans blue (30 mg/kg; Sigma). One minute following the administration of the dye, VEGF (30 ng) or saline was injected intradermally (30 μl total) into the right and left dorsal ear skin, respectively. After 30 min, animals were sacrificed and ears were removed, blotted dry, and weighed. Evans blue content of the ear was evaluated by extraction with 500 μl of formamide for 24 hr at 55°C and measured spectrophotometrically at 610 nm.

Tumor permeability

LLC tumors were grown to approximately 2500 mm^3 on the back of C57BL/6 mice. Mice were treated for 1 hr with the peptides (2.5 mg/kg; i.p.) and were anesthetized (ketamine/xylazine) for the insertion of a polyethylene tube in the left jugular vein. Following peptide treatment, Evans blue (30 mg/kg) was administered through the catheter for 30 min. Mice were sacrificed and perfused with 0.5% paraformaldehyde for 1 min through the left ventricle. Tumors were excised, dried (60°C, 16 hr), and weighed before Evans blue extraction in 1 ml of formamide at 55°C for 16 hr. Evans blue content was quantified by reading at 610 nm in a spectrophotometer. For imaging of vascular leakage, mice bearing LLC tumors were treated as above. Thirty minutes following Evans blue administration, FITC-dextran (MW: 400 kDa, Sigma) was administered (100 mg/kg in PBS) through the jugular vein catheter. The vascular compartment marker was allowed to circulate for 1 min before tumor excision. Tumors were fixed for 48 hr in 10% formalin then sectioned on a vibratome (100 μm sections). Sections were mounted onto glass slides and observed using a Zeiss microscope. Images were obtained using the Openlab image analysis software (Improvision, Lexington, Massachusetts). Images were acquired using a 10× objective field of view under both the TRITC/rhodamine (Evans blue; 300 ms exposure time, 10% gain) and the FITC filters (dextran; 100 ms exposure time, 10% gain). Areas of fluorescence were quantified by evaluating the intensity over background and minimizing the image to a fixed fluorescence intensity level (30 levels over background for Evans blue and 15 levels for FITC). Three images per section were evaluated from three random sections per tumor from at least four different mice per group.

eNOS activity assay

C57BL/6 mice bearing LLC tumors with approximately 2500 mm^3 in size were given either cavtratin or AP-Cav-X (2.5 mg/kg; i.p.) 24 hr and 1 hr before tumors were retrieved by dissection. Tumor tissues were lysed in lysis buffer containing 50 mM Tris-HCl (pH 7.4), 0.1 mM EDTA, 0.1 mM EGTA, 20 mM NaF, 1 mM $Na_4P_2O_7$, 0.3 mg/ml Pefabloc SC, 1 μg/ml leupeptin, 1 μg/ml aprotinin, 2 μg/ml pepstatin A, and 1 mM vanadate. After pulverizing tumor tissues using rotor-stator homogenizer (PowerGen 125, Fisher Scientific), homogenized samples were centrifuged at 1000 rpm for 10 min to remove unbroken cells and tissue. The supernatant was ultracentrifuged at 100,000 × g for 1 hr to separate membrane and cytosolic fractions. The eNOS-enriched membrane fractions were resuspended by dounce homogenization (20 strokes) in the same lysis buffer as above mentioned. eNOS activity assay was performed by conversion of [^{14}C] l-arginine to [^{14}C] l-citrulline. Samples were first assayed to normalize protein concentration. Approximately 800 μg of total protein was used per assay reaction and was diluted in a total volume of 100 μl of activity assay buffer containing 50 mM Tris-HCl (pH 7.5), 0.1 mM EDTA, 0.1 mM EGTA, 100 nM calmodulin (Sigma), 1 mM NADPH (Sigma), 15 μM BH_4 (*6R*-tetrahydro-l-biopterin, Sigma), 8.6 μM L-arginine (Sigma), 1.4 μM [^{14}C] l-arginine (348 mCi/mmol), and 2.5 mM $CaCl_2$ (Sigma) plus or minus 1 mM N^{ω}-nitro-l-arginine methyl ester (L-NAME). All reaction samples were kept on ice until incubation at 37°C for 15 min. The reaction was stopped by adding 1 ml of ice cold stop buffer containing 20 mM HEPES (pH 5.5), 2 mM EDTA, and 2 mM EGTA to each sample. The samples were then passed through Dowex AG50WX8 cation exchange resin and the flow through was counted on a liquid scintillation analyzer.

Immunoprecipitation and Western blotting

For detection of total PECAM and VEGF 165 in tumors, HepG2 tumors at the end of the 14 day peptide treatment were excised and lysed in lysis buffer containing 50 mM Tris-HCl (pH 7.4), 100 mM NaCl, 0.1 mM EGTA, 0.1 mM EDTA, 1% Triton X-100, 1 mM sodium orthovanadate, 20 mM NaF, 1 mM $Na_4P_2O_7$, 1 mM Pefabloc SC, and protease inhibitor cocktail (Roche Diagnostics). Insoluble proteins were removed by centrifugation at 13,000 rpm for 10 min at 4°C. Supernatants were boiled in SDS sample buffer and separated by SDS-PAGE followed by Western blotting for PECAM-1 (Pharmingen), VEGF 165 (Santa Cruz Biotechnologies), and caveolin-1 (Cell Signaling) for loading control. BAECs or EA.hy cells were grown to confluency and serum starved (16 hr) before treatment with either 10 μM of cavtratin, AP-Cav-X (90 min), PP2 (30 min), or 1 mM N^G-monomethyl-l-arginine (L-NMMA) for 45 min followed by 10 ng/ml of VEGF for 5 min (BAEC only).

All cells were washed twice with cold PBS and solubilized with the same lysis buffer as above. Insoluble proteins were removed by centrifugation at

13,000 rpm for 10 min at 4°C. Supernatants were incubated with either Flk-1 (for BAECs) or VE-Cadherin (for EA.hy cells) (Santa Cruz Biotechnology) antibody for 2 hr at 4°C. Protein A Sepharose (Sigma) was then added and incubated for an additional hour. Immune complexes were precipitated by centrifugation, washed three times with lysis buffer, boiled in SDS sample buffer. Samples were then resolved on SDS-PAGE and Western blotted for phosphotyrosine (4G10, Upstate), Flk-1, phospho-Src (P-Tyr 416, Cell Signaling), total Src (Upstate), phospho-caveolin-1 (P-Tyr 14, Cell Signaling), total caveolin-1 (Santa Cruz), or VE-cadherin.

Acknowledgments

We would like to thank Drs. Judah Folkmann and Guillermo Garcia-Cardena for the LLC cell line. This work is supported by grants from the National Institutes of Health (RO1 HL57665, HL61371, and HL64793 to W.C.S.). J.-P.G. was in receipt of a fellowship from the Canadian Institutes of Health Research.

Received: January 17, 2003
Revised: May 29, 2003
Published: July 21, 2003

References

Bates, D.O., Lodwick, D., and Williams, B. (1999). Vascular endothelial growth factor and microvascular permeability. Microcirculation *6*, 83–96.

Bucci, M., Gratton, J.P., Rudic, R.D., Acevedo, L., Roviezzo, F., Cirino, G., and Sessa, W.C. (2000). In vivo delivery of the caveolin-1 scaffolding domain inhibits nitric oxide synthesis and reduces inflammation. Nat. Med. *6*, 1362–1367.

Carmeliet, P., and Collen, D. (2000). Molecular basis of angiogenesis. Role of VEGF and VE-cadherin. Ann. N Y Acad. Sci. *902*, 249–262.

Carmeliet, P., Lampugnani, M.G., Moons, L., Breviario, F., Compernolle, V., Bono, F., Balconi, G., Spagnuolo, R., Oostuyse, B., Dewerchin, M., et al. (1999). Targeted deficiency or cytosolic truncation of the VE-cadherin gene in mice impairs VEGF-mediated endothelial survival and angiogenesis. Cell *98*, 147–157.

Claffey, K.P., Abrams, K., Shih, S.C., Brown, L.F., Mullen, A., and Keough, M. (2001). Fibroblast growth factor 2 activation of stromal cell vascular endothelial growth factor expression and angiogenesis. Lab. Invest. *81*, 61–75.

Dvorak, H.F., Sioussat, T.M., Brown, L.F., Berse, B., Nagy, J.A., Sotrel, A., Manseau, E.J., Van de Water, L., and Senger, D.R. (1991). Distribution of vascular permeability factor (vascular endothelial growth factor) in tumors: concentration in tumor blood vessels. J. Exp. Med. *174*, 1275–1278.

Dvorak, H.F., Nagy, J.A., Dvorak, J.T., and Dvorak, A.M. (1988). Identification and characterization of the blood vessels of solid tumors that are leaky to circulating macromolecules. Am. J. Pathol. *133*, 95–109.

Eliceiri, B.P., Paul, R., Schwartzberg, P.L., Hood, J.D., Leng, J., and Cheresh, D.A. (1999). Selective requirement for Src kinases during VEGF-induced angiogenesis and vascular permeability. Mol. Cell *4*, 915–924.

Fukumura, D., Gohongi, T., Kadambi, A., Izumi, Y., Ang, J., Yun, C.O., Buerk, D.G., Huang, P.L., and Jain, R.K. (2001). Predominant role of endothelial nitric oxide synthase in vascular endothelial growth factor-induced angiogenesis and vascular permeability. Proc. Natl. Acad. Sci. USA *98*, 2604–2609.

Garcia-Cardena, G., Martasek, P., Masters, B.S., Skidd, P.M., Couet, J., Li, S., Lisanti, M.P., and Sessa, W.C. (1997). Dissecting the interaction between nitric oxide synthase (NOS) and caveolin. Functional significance of the nos caveolin binding domain in vivo. J. Biol. Chem. *272*, 25437–25440.

Labrecque, L., Royal, I., Surprenant, D.S., Patterson, C., Gingras, D., and Beliveau, R. (2003). Regulation of vascular endothelial growth factor receptor-2 activity by caveolin-1 and plasma membrane cholesterol. Mol. Biol. Cell *14*, 334–347.

Lindsberg, P.J., Siren, A.L., and Hallenbeck, J.M. (1997). Microvascular perfusion during focal vasogenic brain edema: a scanning laser fluorescence microscopy study. Microvasc. Res. *53*, 92–103.

Matsumoto, T., and Claesson-Welsh, L. (2001). VEGF receptor signal transduction. Sci STKE *112*, RE21.

Mauceri, H.J., Hanna, N.N., Beckett, M.A., Gorski, D.H., Staba, M.J., Stellato, K.A., Bigelow, K., Heimann, R., Gately, S., Dhanabal, M., et al. (1998). Combined effects of angiostatin and ionizing radiation in antitumour therapy. Nature *394*, 287–291.

Michel, C.C., and Curry, F.E. (1999). Microvascular permeability. Physiol. Rev. *79*, 703–761.

Michel, J.B., Feron, O., Sacks, D., and Michel, T. (1997). Reciprocal regulation of endothelial nitric-oxide synthase by Ca2+- calmodulin and caveolin. J. Biol. Chem. *272*, 15583–15586.

Murohara, T., Asahara, T., Silver, M., Bauters, C., Masuda, H., Kalka, C., Kearney, M., Chen, D., Symes, J.F., Fishman, M.C., et al. (1998a). Nitric oxide synthase modulates angiogenesis in response to tissue ischemia. J. Clin. Invest. *101*, 2567–2578.

Murohara, T., Horowitz, J.R., Silver, M., Tsurumi, Y., Chen, D., Sullivan, A., and Isner, J.M. (1998b). Vascular endothelial growth factor/vascular permeability factor enhances vascular permeability via nitric oxide and prostacyclin. Circulation *97*, 99–107.

Papapetropoulos, A., Garcia-Cardena, G., Madri, J.A., and Sessa, W.C. (1997). Nitric oxide production contributes to the angiogenic properties of vascular endothelial growth factor in human endothelial cells. J. Clin. Invest. *100*, 3131–3139.

Schubert, W., Frank, P.G., Woodman, S.E., Hyogo, H., Cohen, D.E., Chow, C.W., and Lisanti, M.P. (2002). Microvascular hyperpermeability in caveolin-1 (−/−) knock-out mice. Treatment with a specific nitric-oxide synthase inhibitor, L-name, restores normal microvascular permeability in Cav-1 null mice. J. Biol. Chem. *277*, 40091–40098.

Stacker, S.A., Achen, M.G., Jussila, L., Baldwin, M.E., and Alitalo, K. (2002). Lymphangiogenesis and cancer metastasis. Nat. Rev. Cancer *2*, 573–583.

Ziche, M., Morbidelli, L., Choudhuri, R., Zhang, H.T., Donnini, S., Granger, H.J., and Bicknell, R. (1997). Nitric oxide synthase lies downstream from vascular endothelial growth factor-induced but not basic fibroblast growth factor-induced angiogenesis. J. Clin. Invest. *99*, 2625–2634.